ing over $Q$, a process known as "water-filling" (*2*). This case can also be handled within our framework.


**References and Notes**

1. T. S. Rappaport, *Wireless Communications, Principles and Practice* (Prentice-Hall, Englewood Cliffs, NJ, 1996).
2. T. M. Cover and J. A. Thomas, *Elements of Information Theory* (Wiley, New York, 1991); S. Kullback, *Information Theory and Statistics* (Wiley, New York, 1959).
3. G. J. Foschini and M. Gans, *Wireless Personal Commun.* **6**, 311 (1998).
4. I. E. Telatar, *Eur. Trans. Telecommun.*, in press.
5. C. E. Shannon, *Bell Syst. Tech. J.* **27**, 379, 623 (1948).
6. B. L. Altshuler, P. A. Lee, R. A. Webb, Eds., *Mesoscopic Phenomena in Solids* (North-Holland, New York, 1991).
7. E. Akkermans, G. Montambaux, J.-L. Pichard, J. Zinn-Justin, Eds., *Mesoscopic Quantum Physics* (Elsevier, New York, 1995).
8. M. J. Stephen, in (*6*), pp. 81–106.
9. M. C. W. van Rossum and Th. M. Nieuwenhuizen, *Rev. Mod. Phys.* **71**, 313 (1999).
10. D. Ullmo and H. U. Baranger, *IEEE Trans. Veh. Technol.* **48**, 947 (1999).
11. A. M. Sengupta and P. P. Mitra, *Phys. Rev. E* **60**, 3389 (1999).
12. M. J. Stephen and G. Cwilich, *Phys. Rev. B* **34**, 7564 (1986).
13. E. Biglieri, J. Proakis, S. Shamai (Shitz), *IEEE Trans. Inf. Theory* **44**, 2619 (1998).
14. J. G. Foschini, M. Gans, D. Shiu, J. M. Kahn, *IEEE Trans. Commun.*, in press.
15. Formally, we pose this information theory problem as follows. The received signal vector is $y = Gx + \eta$ where $x$ is the transmitted vector and $\eta$ is the noise vector. Thus, the channel is defined by $p(\{G,y\}|x) = p(G)p(y|\{G,x\})$ where $p(G) \propto \exp[-n_T/2S\ \mathrm{Tr}(GT^{-1}G^{\dagger}R^{-1})]$ gives $G$ the proper statistics as defined by Eq. 1, and $p(y|\{G,x\}) \propto \exp(-1/2N|y - Gx|^2)$ describes independent noise of average power $N$ in each component of $\eta$. The capacity as shown in Eq. 3 is then the mutual information $I(\{G,y\};x)$ maximized over all possible $p(x)$ transmitted.
16. A. M. Sengupta and P. P. Mitra, Bell Labs Memo 11111-990318-05.


17. We thank G. J. Foschini, M. Gans, and B. I. Halperin for illuminating discussions.

26 August 1999; accepted 22 November 1999

# Direct Observation of Dynamical Heterogeneities in Colloidal Hard-Sphere Suspensions

**Willem K. Kegel[1] and Alfons van Blaaderen[1,2]**

**The real-space dynamics in a model system of colloidal hard spheres was studied by means of time-resolved fluorescence confocal scanning microscopy. Direct experimental evidence for the presence of dynamical heterogeneities in a dense liquid was obtained from an analysis of particle trajectories in two-dimensional slices of the bulk sample. These heterogeneities manifest themselves as a non-Gaussian probability distribution of particle displacements and also affect the onset of long-time diffusive behavior.**

Many liquids can be transformed into a glass, a solid phase without long-range positional order, by cooling them rapidly below their freezing temperature (*1, 2*). The change in molecular relaxation processes upon approaching the glass transition continues to be the subject of much experimental and theoretical work [for a recent review see (*3*)]. This change reflects the increase of correlations of the particle movements upon approaching the glass transition. However, such relaxation processes are not only of interest from a fundamental viewpoint: The nature and time scales of these processes determine the (kinetic) stability of a glass (relative to the crystalline state) and its mechanical properties.

An important observation in many molecular glass-forming liquids is a nonexponential decay of (ensemble-averaged) time correlation functions [see (*4*) and references therein]. Both computer simulation and indirect experimental evidence [for example, (*5*)] suggest that a superposition of different relaxation processes, or dynamic heterogeneity, underlies this nonexponential behavior. Molecular dynamics simulations have given direct evidence for dynamical heterogeneities (*6, 7*), and a Monte Carlo simulation of hard spheres, which focused on three-time correlations of single particles (*8*), also indicates (albeit indirectly) that dynamical heterogeneities occur.

In recent studies on colloidal systems, the dynamics of tracer particles was investigated by optical microscopy (*9*) and by dynamic light scattering (*10*). In both studies, deviations of the displacement distribution function from Gaussian behavior were observed. However, dynamical heterogeneities were not observed directly in these experiments. Colloidal systems may be regarded as collections of "superatoms" in which the interaction potential can be tailored (*11*), for example, by changing the solvent quality. During the past decade, they have also been used as model systems to study the glass transition (*12*).

Here, we investigated the nature of dynamical heterogeneities for the simplest possible experimental (model) system of interacting particles: hard colloidal spheres. We used fluorescent confocal scanning laser microscopy to obtain time series of digital images of the colloidal particles, in slices in the bulk of the sample. The data from these images enable us to address the question of how these heterogeneities are manifested in (real-space) correlation functions.

Colloidal particles that could be observed directly by microscopy were developed in our laboratory. They are of a core-shell nature and can be matched for (mass) density and for refractive index (*13*). The particles consist of a core of silica with a fluorescent dye (fluorescein isothiocyanate) (*14*), 450 nm in diameter, covered with a large shell of polymethylmethacrylate (PMMA) with a steric stabilizing layer (~10 nm thick) of 12-polyhydroxystearic acid (PHS) that is covalently linked to the PMMA (*15, 16*). The particles were dispersed in a mixture of tetralin, decalin, and carbon tetrachloride in which the particles are almost matched with respect to refractive index and density. In this solvent mixture, the diameter of the particles is 1.40 μm and the size polydispersity is ~6%. This relatively large polydispersity inhibits crystallization (above the freezing volume fraction of 0.494) considerably: Months elapsed before crystallites formed. From the location of the coexisting fluid-crystal volume fractions and from light scattering studies, it could be concluded that the particles behave as hard spheres. This conclusion is corroborated by the shape of the pair correlation or radial distribution function (see below) and by the independence of the location of the first peak on the volume fraction of the spheres.

The volume fraction of the particles where no movement was observed (except for a few "rattlers," trapped particles that are not immobilized) was set at 0.66. This density coincides with the volume fraction at random close packing of 6% polydisperse hard spheres (*17*). All volume fractions are defined relative to this point. Because of the core-shell character of the particles, time-dependent coordinates of their centers could be obtained with high accuracy using proce-

[1]Van't Hoff Laboratory for Physical and Colloid Chemistry, Debye Institute, Utrecht University, Padualaan 8, 3584 CH Utrecht, Netherlands. [2]Institute for Atomic and Molecular Physics, Stichting voor Fundamenteel Onderzoek der Materie (FOM), Kruislaan 407, 1098 SJ Amsterdam, Netherlands.

dures similar to those described in (*18*).

The thickness of the slices that were analyzed is ~0.5 particle diameters, which leads to errors in the in-plane structural correlation functions at distances comparable to this thickness (*19*). We avoided this situation by reducing the slice thickness if the correlation functions were evaluated at small distances. This reduction in slice thickness was achieved by discriminating particles that were too far from the focal plane on the basis of their fluorescence intensity. We checked this procedure by comparing the in-plane pair correlation function, $g(r)$, with the full three-dimensional (3D) pair correlation function of the same system [using the method in (*20*)]. Very good agreement was observed.

The positions of the centers of the spheres over 100 time steps are plotted in Fig. 1, A to D, for several volume fractions. As shown experimentally in (*21*), hard spheres undergo a freezing transition at volume fraction $\phi = 0.494$. For $0.494 < \phi < 0.545$, crystal and fluid coexist, and above $\phi = 0.545$, the thermodynamically stable state of hard spheres is a crystal. At $\phi \approx 0.57$, a glass transition has been observed. All samples studied here are in a (metastable) fluid state. Here and below, all distances are given in units of the diameter $D$ of the spheres, and time is in units of the Brownian time, the time a sphere at infinite dilution takes to diffuse over its own diameter, $\tau_b = D^2/6D_0 = 1.6092$ s, where $D_0$ is the (Brownian) diffusion coefficient at infinite dilution. The systems with $\phi = 0.57$ and $\phi = 0.60$ clearly show regions of high mobility in a "sea" of more slowly moving particles. These high-mobility regions are narrow but quite extended (that is, not compact), and the trajectories qualitatively look like those found in computer simulations of 2D liquids (*6*). At later times, the high-mobility regions appear at different locations. We also show the pair correlation function (being proportional to the probability of observing a sphere center a distance $r$ away from a given sphere center) of the system with $\phi = 0.60$, which shows typical features of dense fluids (Fig. 1E) (*20, 22*).

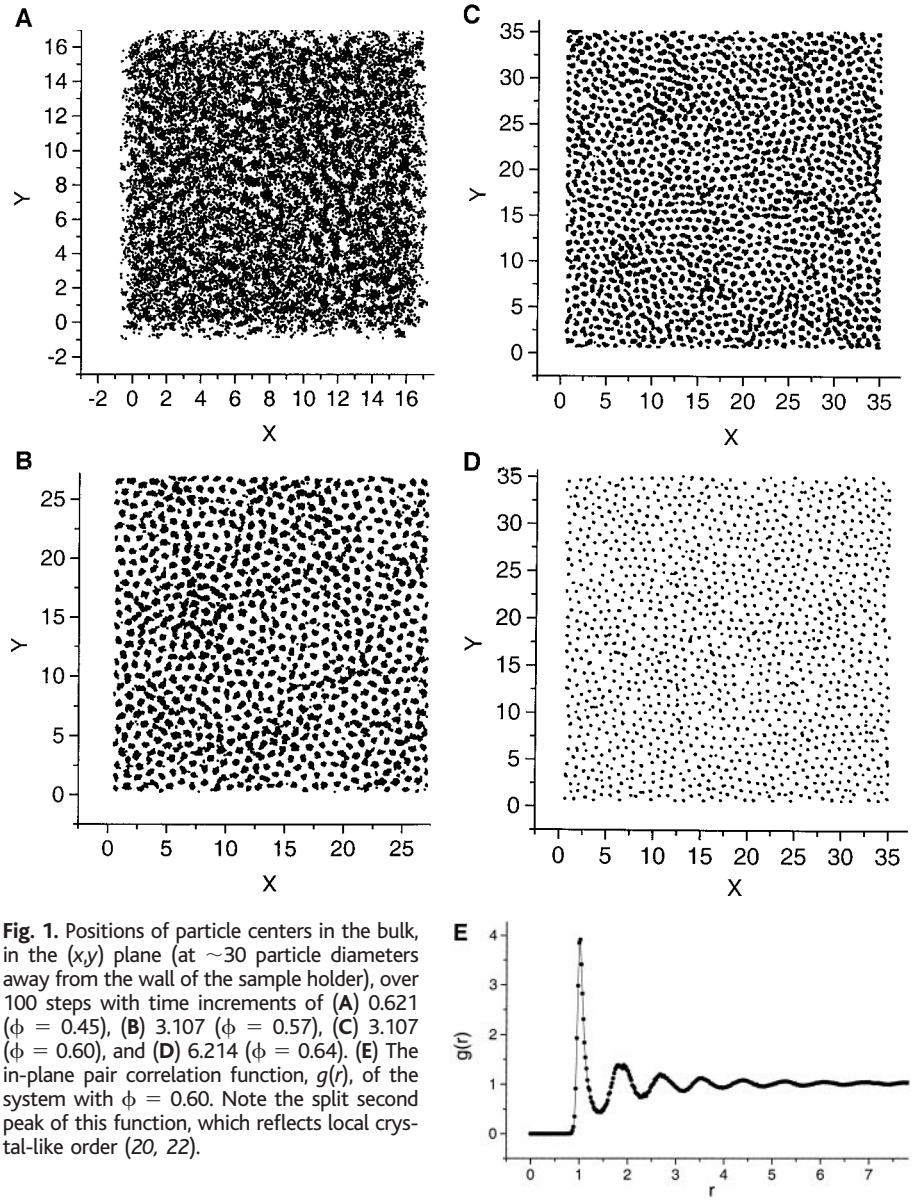


**Fig. 1.** Positions of particle centers in the bulk, in the $(x,y)$ plane (at ~30 particle diameters away from the wall of the sample holder), over 100 steps with time increments of (**A**) 0.621 ($\phi = 0.45$), (**B**) 3.107 ($\phi = 0.57$), (**C**) 3.107 ($\phi = 0.60$), and (**D**) 6.214 ($\phi = 0.64$). (**E**) The in-plane pair correlation function, $g(r)$, of the system with $\phi = 0.60$. Note the split second peak of this function, which reflects local crystal-like order (*20, 22*).

The dynamical heterogeneities are manifested as a non-Gaussian self-part of the van Hove correlation function, $G_s(x,\tau)$. This function is the equilibrium, canonically averaged probability distribution of displacements (*23*):

$$G_s(x,\tau) = \frac{1}{N}\left\langle \sum_{i=1}^{N} \delta[x + x_i(0) - x_i(\tau)] \right\rangle = \frac{N(x,\tau)}{N} \quad (1)$$

where $x$ is the distance from a given particle center along the $x$ coordinate. Choosing a radial distance would not add information. $N(x,\tau)$ is the number of particles that move a distance between $x$ and $(x + dx)$ in a time interval $\tau$, and $N$ is the number of particles. The angle brackets denote canonical averaging. The function $G_s(x,\tau = 3.1)$ for the system with $\phi = 0.55$ clearly deviates from a Gaussian (Fig. 2). The lowest order deviation of $G_s(x,\tau)$ from a Gaussian is quantified by

$$\alpha_2(\tau) = \frac{\langle x^4(\tau)\rangle}{3\langle x^2(\tau)\rangle^2} - 1 \quad (2)$$

(*24*) with

$$\langle x^b(\tau)\rangle = \sum_{i=1}^{N} x^b(\tau) G_s(x,\tau) \quad (3)$$

It is zero if $G_s(x,\tau)$ is strictly Gaussian. To improve statistics, we redefine $\langle x^b\rangle$ as $(\langle x^b\rangle + \langle y^b\rangle)/2$, where $x$ and $y$ are perpendicular axes in a plane. We computed the values of $\alpha_2$ for all displacements and for the slowest and fastest subsets of $G_s(x,\tau)$. These subsets always have a significantly smaller non-Gaus-

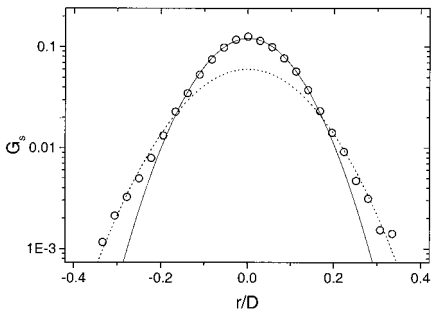


**Fig. 2.** Self-part of the van Hove correlation function, $G_s(x,\tau = 3.1)$, for a system with $\phi = 0.55$. The analyses involved a total of $5 \times 10^4$ displacements (○). The solid line is a Gaussian fit to the data. The dashed line is a Gaussian fit to the data that belong to a fast subset, defined as absolute displacements larger than 0.175.

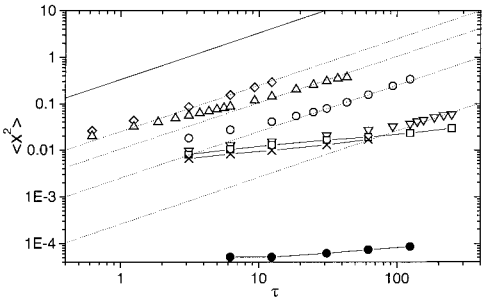


**Fig. 3.** Mean squared displacement versus Brownian time for systems with $\phi = 0.45$ (◇), $\phi = 0.48$ (△), $\phi = 0.52$ (○), $\phi = 0.55$ (▽), $\phi = 0.57$ (□), $\phi = 0.60$ (×), and $\phi = 0.64$ (●). The solid line corresponds to unrestricted diffusion, where $\langle x^2(\tau = 1)\rangle = 1/3$. Dotted lines signify the long-time diffusion regime, where $\langle x^2(\tau)\rangle = a\tau$. The values of $a$ that were used, with increasing volume fractions, are 0.025, 0.0105, 0.0025, and 0.00026.

sian parameter $\alpha_2$ than that of the full distribution. This result reflects the observation that $G_s(x,\tau)$ could reasonably well be described by a sum of two Gaussians: a wide one for the most mobile fraction of the particles, and a narrow one for the slowest fraction. This behavior is illustrated in Fig. 2, where we define the fast subset somewhat arbitrarily as particles with absolute displacements larger than 0.175 (corresponding to the fastest 10% of the particle population). For the full distribution, we find $\alpha_2 = 1.14 \pm 0.23$, whereas for the fast subset we have $\alpha_2 = 0.00 \pm 0.17$. The result of the Gaussian fit to the fast subset is also shown in Fig. 2. Thus, the particle population consists of subpopulations significantly faster and significantly slower than would be expected from a single Gaussian distribution. A significantly smaller non-Gaussian parameter was also found when those regions where no apparent fast particles were present in Fig. 1, B and C, were selected and analyzed. This clearly demonstrates [as also suggested by computer simulations; see for example (*6, 7*)] that the non-Gaussian behavior of the self-part of the van Hove correlation function reflects the dynamical heterogeneities present in the system and is not an "intrinsic" property of the particles, nor is it caused by statistical errors in the tails of the distribution.

At what stage in the relaxation process is the non-Gaussian effect most prominent? We studied volume fractions of the spheres from $\phi = 0.45$ (below the freezing density) to $\phi = 0.64$ (close to random close packing). The mean squared displacements as a function of the time interval are shown in Fig. 3. Diffusive behavior is defined by $\langle x^2(\tau)\rangle = 2D_s\tau$, where $D_s$ is the self-diffusion coefficient. At smaller values of $\tau$ that are still large enough so that many collisions with solvent molecules have taken place, $D_s$ represents the short-time self-diffusion coefficient. It becomes the long-time diffusion coefficient when $\tau \rightarrow \infty$ (*25*). The short-time diffusion regime is not accessible with the scanning technique because of the finite scanning speed. The systems with volume fractions from 0.45 to 0.55 show nondiffusive behavior at (relatively) short times—this is the regime where the particles experience "caging" (or temporary localization) because of the presence of their neighbors—followed by an apparent diffusive regime, indicated by a unit slope in Fig. 3. The Brownian time at which the onset of diffusion is apparent is comparable to what was found by dynamic light scattering (*10*). The behavior of the systems with $\phi \geq 0.57$ is nondiffusive over all the time intervals studied. This is approximately the volume fraction of hard spheres where a glass transition is found (*21*): It is where the intrinsic system relaxation time crosses an experimental time window.

A plot of the values of the non-Gaussian parameter as a function of the mean squared displacement (Fig. 4) enables us to compare the systems when their particles move over certain distances. It follows from Fig. 4 that $\alpha_2$ tends to pass through a maximum (which does not seem to be reached in the more concentrated systems) as a function of the mean squared displacement, but except for the system with $\phi = 0.55$, the variation of $\alpha_2$ is hardly significant. Still, the results are compatible with those found by dynamic light scattering (*10*) and computer simulations (*7*); that is, the location of the maxima is at a relatively late stage in the relaxation process. The maximum value of $\alpha_2$ in Fig. 4 significantly increases when the glass transition is approached, which is also in accord with the studies referred to above. Moreover, these results are in qualitative agreement with recent predictions from mode-coupling theory (*26*) for hard spheres, although quantitatively the values found here are greater than the predicted values by as much as an order of magnitude. The increasing value of $\alpha_2$ qualitatively explains why diffusive behavior (Fig. 3) is observed at decreasing values of $\langle x^2\rangle$ when the volume fraction is increased (that is, a faster decrease than the decrease in average particle distance): $\langle x^2\rangle$ is particularly sensitive to the most mobile fraction of particles. Either this fraction or its mobility relative to the mean mobility, or both, are expected to increase with $\alpha_2$ because this parameter measures widening in the tails of the displacement distribution. Our data indicate increasing relative mobilities. Thus, the apparent diffusive behavior of the systems with high volume fractions may only reflect a property of a minority of the particle population.

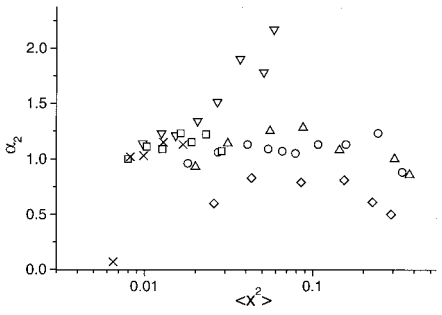
2.0
1.5
1.0
0.5
0.0
α₂
0.01
0.1
<x²>
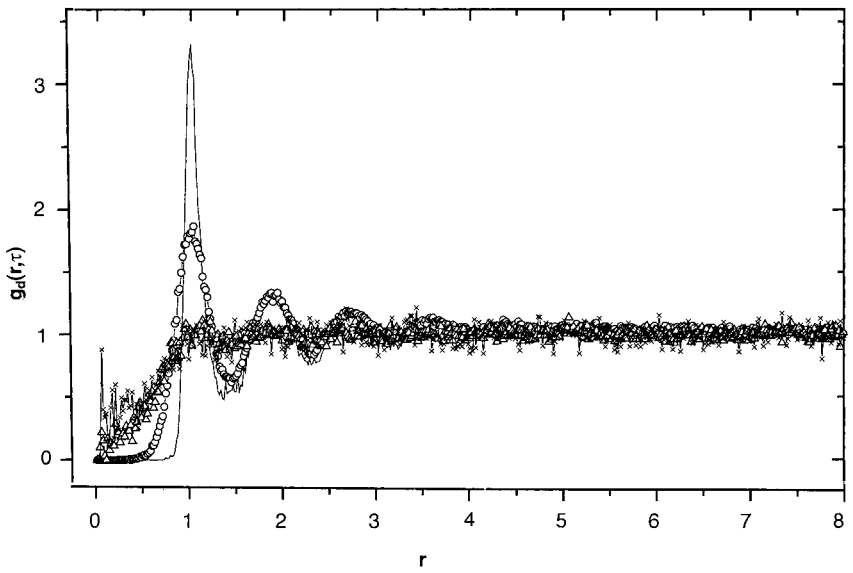


**Fig. 4.** Values of the non-Gaussian parameter $\alpha_2$ as a function of the mean squared displacement. Symbols are as in Fig. 3. The uncertainty in the values of $\alpha_2$ is ~20%.

**Fig. 5.** $g_d(r,\tau) = G_d(r,\tau)/\rho$, where $G_d(r,\tau)$ is the distinct part of the van Hove correlation function, versus $r$ for $\phi = 0.52$, at $\tau = 9.3$ (○), 74.6 (△), and 121.2 (×). The solid line is the pair correlation function $g(r) = g_d(r,\tau = 0)$.

This scenario is verified by the behavior of the distinct part of the van Hove correlation function:

$$G_d(r,\tau) = \frac{1}{N}\left\langle \sum\sum_{i\neq j}^{N} \delta[r + r_j(0) - r_i(\tau)] \right\rangle \quad (4)$$

This function is proportional to the probability of finding a particle $i \neq j$ in a region $dr$ around $r$ at time $\tau$, provided that a particle $j$ was at the origin at $\tau = 0$. In Fig. 5, we plotted $g_d(r,\tau) = G_d(r,\tau)/\rho$, where $\rho$ is the in-plane number density, for the system with $\phi = 0.52$ at several times. Even at times where diffusive behavior is observed (compare with Fig. 3), there is a considerably smaller probability of finding a particle in the region $0 < r < 1$ relative to finding it elsewhere. The same trend was observed in the other systems with $\phi \leq 0.52$ (*27*). This result demonstrates that the onset of the diffusive regime reflects the behavior of the more mobile fraction of particles: Diffusive behavior is apparent even though the systems bear significant memory of their local structure.

We have shown that a system in which only excluded volume interactions operate exhibits dynamical heterogeneities. These heterogeneities manifest themselves in a non-Gaussian self-part of the van Hove correlation function and influence the onset of apparent long-time diffusion.

**References and Notes**


1. P. G. Debenedetti, *Metastable Liquids* (Princeton Univ. Press, Princeton, NJ, 1996).
2. C. A. Angell, *Science* **267**, 1924 (1995).
3. H. Sillescu, *J. Non-Cryst. Solids* **243**, 81 (1999).
4. M. T. Cicerone and M. D. Ediger, *J. Chem. Phys.* **103**, 5684 (1996).
5. K. Schmidt-Rohr and H. W. Spiess, *Phys. Rev. Lett.* **66**, 3020 (1991).
6. M. Hurley and P. Harrowell, *Phys. Rev. E* **52**, 1694 (1995).
7. W. Kob *et al.*, *Phys. Rev. Lett.* **79**, 2827 (1997).
8. B. Doliwa and A. Heuer, *Phys. Rev. Lett.* **80**, 4915 (1998).
9. A. Kasper, E. Bartch, H. Sillescu, *Langmuir* **14**, 5004 (1998).
10. T. C. Mortensen and W. van Megen, in *Slow Dynamics in Complex Systems*, M. Tokuyama and I. Oppenheim, Eds. (American Institute of Physics, Woodbury, NY, 1998), p. 3.
11. W. Poon, P. N. Pusey, H. N. W. Lekkerkerker, *Phys. World* (April), 27 (1996).
12. W. van Megen and S. M. Underwood, *Nature* **362**, 616 (1993).
13. A. van Blaaderen, G. Bosma, Z. Dogic, C. Pathmamanoharan, W. K. Kegel, in preparation.
14. A. van Blaaderen and A. Vrij, *Langmuir* **8**, 2921 (1992).
15. L. Antl *et al.*, *Colloid Surf.* **17**, 67 (1986).
16. C. Pathmamanoharan, C. Slob, H. N. W. Lekkerkerker, *Colloid Polymer Sci.* **267**, 448 (1989).
17. W. Schaertl and H. Sillescu, *J. Stat. Phys.* **77**, 1007 (1994).
18. J. C. Crocker and D. G. Grier, *J. Colloid Interface Sci.* **179**, 298 (1996).
19. J. Bongers *et al.*, *J. Chem. Phys.* **108**, 9937 (1998).
20. A. van Blaaderen and P. Wiltzius, *Science* **270**, 1177 (1995).
21. P. N. Pusey and W. van Megen, *Nature* **320**, 340 (1986).
22. T. M. Truskett *et al.*, *Phys. Rev. E* **58**, 3083 (1998).
23. J. P. Hansen and I. R. McDonald, *Theory of Simple Liquids* (Academic Press, London, 1986).
24. B. R. A. Nijboer and A. Rahman, *Physica* **32**, 415 (1966).
25. J. K. G. Dhont, in *An Introduction to Dynamics of Colloids*, D. Möbius and R. Miller, Eds. (Elsevier, Amsterdam, 1996), pp. 327–329.
26. M. Fuchs, W. Götze, M. R. Mayr, *Phys. Rev. E* **58**, 3384 (1998).
27. W. K. Kegel and A. van Blaaderen, data not shown.



28. We thank G. Bosma, Z. Dogic, and C. Pathmamanoharan for their contribution in preparing the core-shell particles; J. Hoogenboom for computing $g(r)$ in three dimensions; H. Lekkerkerker for many discussions during initialization of this work and for continuous interest; and G. Koenderink and D. Frenkel for comments on the manuscript. W.K.K. thanks P. Harrowell for enlightening discussions and correspondence. Supported by the Royal Dutch Academy of Arts and Sciences (W.K.K.) and by FOM, which is part of the Netherlands Organization for Scientific Research.

16 August 1999; accepted 15 November 1999


# Formation of Cyclic Water Hexamer in Liquid Helium: The Smallest Piece of Ice


**K. Nauta and R. E. Miller***



**The cyclic water hexamer, a higher energy isomer than the cage structure previously characterized in the gas phase, was formed in liquid helium droplets and studied with infrared spectroscopy. This isomer is formed selectively as a result of unique cluster growth processes in liquid helium. The experimental results indicate that the cyclic hexamer is formed by insertion of water molecules into smaller preformed cyclic complexes and that the rapid quenching provided by the liquid helium inhibits its rearrangement to the more stable cage structure.**


The study of neutral water clusters holds considerable promise for obtaining a molecular level description of the properties of bulk water. Through the investigation of progressively larger clusters, it is becoming possible to systematically probe the various n-body terms in the corresponding intermolecular potential. Intense experimental (*1–6*) and theoretical (*7–10*) work has focused on the detailed characterization of the water dimer, trimer, tetramer, and larger clusters. The structural landscape associated with the larger clusters is quite rich, and theoretical studies have revealed many different local minima on the associated potential energy surfaces that correspond to a range of structural isomers. Many of these isomers are reminiscent of transient structures that appear in liquid water and the tetrahedral network of ice, which suggests that their study can provide insights into the bulk properties of water.

Despite this rich landscape, the current experimental studies of small water clusters have revealed only a single (the most stable) isomer for each cluster size, which greatly limits the configuration space that can be explored in this way. In the present study, we use superfluid liquid helium as a growth medium to access a different portion of the structural landscape and in particular report the experimental observation of the cyclic water hexamer. The importance of this observation can be appreciated by noting that the cyclic hexamer is one of the prominent morphologies found in computer simulations of liquid water and is the structural motif for ice $I_h$ (*11*, *12*). The ab initio structure of the cyclic water hexamer (*9*, *13*, *14*) is shown in Fig. 1, along with the cage isomer characterized previously by Saykally and coworkers (*1*, *2*).

The apparatus used in the present study has been discussed in some detail previously (*15*). Helium droplets are formed by expanding ultrapure helium gas from a pressure of ~60 bar through a 5-μm-diameter nozzle that is cooled to 19 to 22 K with a closed-cycle helium refrigerator. These droplets pass through the pick-up chamber, which was maintained at a variable water pressure to control the number of molecules they capture. Cluster formation within the droplet is ensured if more than one water molecule is captured because the interactions between molecules are far stronger than those between water and helium.

Before discussing the experimental results, it is important to consider how cluster growth in liquid helium differs from homogeneous nucleation in a free jet expansion and why the two methods might be expected to give rise to different structures. In a free jet, nucleation occurs early in the expansion, and the clusters subsequently cool by two-body collisions. This relatively slow cooling (compared with that in liquid helium) facilitates the annealing of clusters


Department of Chemistry, University of North Carolina, Chapel Hill, NC 27599, USA.

*To whom correspondence should be addressed. E-mail: remiller@unc.edu